Showcasing research from Micro/nanoscale thermofluidics research group of Professor Masahiro Motosuke, Tokyo University of Science, Tokyo, Japan.

Continuous-flow electrorotation (cROT): improved throughput characterization for dielectric properties of cancer cells

This study presents a novel assay platform, continuous-flow electrorotation (cROT), a label-free characterization technique for the electric properties of cancer cells under continuous flow conditions. The electrode array on the top and bottom substrates torques the cells with a vertical rotation axis to the main flow in the microchannel. The proposed cROT device can perform simultaneous measurements of electric properties, cytoplasm conductivity and membrane permittivity, for multiple cells with an improved throughput.

ROYAL SOCIETY
OF **CHEMISTRY**

rsc.li/loc

Registered charity number: 207890

Check for updates

Continuous-flow electrorotation (cROT): improved throughput characterization for dielectric properties of cancer cells†

Kazuma Yoda,[a] Yoshiyasu Ichikawa [iD][bc] and Masahiro Motosuke [iD] *[bc]

This paper presents the concept of a newly developed high-throughput measurement device for determining the dielectric properties of cancer cells. The proposed continuous-flow electrorotation (cROT) device can induce electrorotation (ROT) with vertical rotation using two sets of interdigitated electrodes on the top and bottom substrates to torque the cells. In the developed device, multiple rotating cells flowing in a microchannel are aligned between electrodes using dielectrophoresis. This allows for the measurement of the rotational behavior of the cells with continuous flow, resulting in a significant improvement in throughput compared to the conventional ROT devices reported previously. The dielectric properties, permittivity of the cell membrane and conductivity of the cell cytoplasm, of HeLa cells obtained by simultaneous measurements using the developed cROT device were 9.13 ± 1.02 and 0.93 ± 0.10 S m^{-1}, respectively. Moreover, the measurement throughput was successfully increased to 2700 cells per h using the cROT technique.

1. Introduction

Recent advances in medical technology have improved surgical procedures, radiation therapy, and chemotherapy. However, cancer is still associated with a high mortality rate mainly due to the metastasis of cancer and the expression of drug resistance.[1–6] These features disrupt cancer treatment, reducing its efficacy and leading to recurrence.[7] Therefore, it is essential to monitor the status of cancer.[8–10] Techniques using the dielectric properties of cancer cells, such as permittivity and conductivity, have been developed as non-invasive and simple methods for cancer monitoring.[11–18]

The dielectric properties of cancer cells reflect cancer types and their status of drug resistance.[1,3,12,13] Alazzam *et al.* reported the microfluidic separation of circulating tumor cells (CTCs) from blood utilizing these characteristics.[19] Compared to normal blood cells, CTCs show different dielectric properties, which have different polarities of dielectrophoresis (DEP) forces in a non-uniform electric field. In addition to CTCs, exosomes and circulating tumor DNA (ctDNA) have recently been used as biomarkers, showing the possibility of separation and collection by DEP.[20–22] To realize applications for advanced cancer diagnosis and monitoring using electrical properties, it is necessary to acquire the properties of cancer cells and establish their database in advance. Thus, methods for determining the electrical properties of cancer cells are in high demand.[23–25]

Electrorotation (ROT) has been proposed as a non-invasive technique to determine the dielectric properties of cells. ROT is a phenomenon in which cells rotate depending on their dielectric properties, and the permittivity and conductivity of individual cells can be determined from their rotational behavior.[13,23] ROT can provide the dielectric properties of cancer cells without contact between the cell and the electrode; thus, it is not affected by the shape of the electrode or its contact resistance. As shown in Fig. 1(a), a rotating electric field was generated by applying four AC voltages with a phase difference of 90° using four electrodes, #1–4. Consequently, the cell placed at the center of the electrodes rotates owing to the rotating electric field. The angular velocity of the rotation varied depending on the frequency of the applied AC electric field. The type and state of the cells can be characterized by analyzing the frequency-dependent angular velocity. To determine the dielectric properties of a cell by ROT, individual cells must be placed at the center of each electrode when measuring a single cell or multiple cells simultaneously. Because negative DEP can act as a force on the cell in the direction away from the electrode, many

a Department of Mechanical Engineering, Graduate School of Engineering, Tokyo University of Science, Japan

b Department of Mechanical Engineering, Faculty of Engineering, Tokyo University of Science, Japan. E-mail: mot@rs.tus.ac.jp

c Water Frontier Research Center, Research Institute for Science and Technology, Tokyo University of Science, Japan

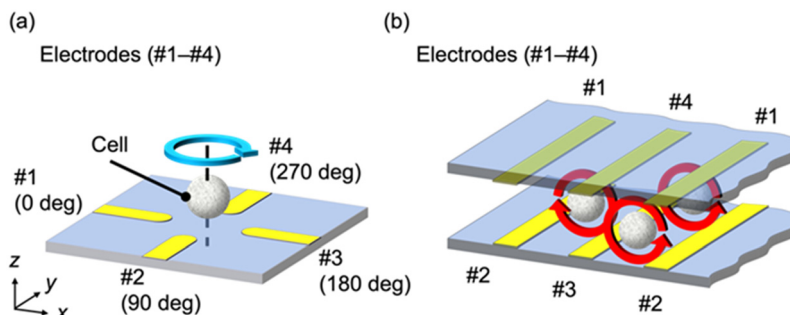† Electronic supplementary information (ESI) available. See DOI: https://doi.org/10.1039/d3lc00301a

Fig. 1 Schematic of a cell rotation movement in a rotating AC electric field for (a) conventional ROT and (b) newly developed cROT. In conventional ROT in (a), when AC voltage is applied to four electrodes arranged in the plane of observation (xy), each with a phase difference of 90°, the cell receives a torque and rotates. Notably, the rotational direction of cells differs in (a) and (b). Since the rotation speed of the cell depends on the dielectric properties of the cell, the dielectric properties of the cell can be determined from its rotation behavior. In the developed electrode structure of cROT in (b), multiple cells rotate at the same time in the same system with the electrode array located in the xz-section. Moreover, cells at any position between the electrodes in the y-direction can receive the same rotational torque. The electrode rows are also located in the x-direction, and the cells can be arranged in a two-dimensional (xy-plane) array; thus, their rotational behavior can be measured.

previous studies exploited DEP with ROT to capture target cells.[23,26–30] This method enabled the measurement of the stable rotation behavior of a cell because the DEP force levitates the cells and they rotate without contact with the electrode or substrate. However, some cells were not appropriately captured or the measurement was disrupted by other irruptive cells during analysis. Therefore, it is necessary to perform the capture operation for the measurement of a large number of cells.[17–19] In addition, high voltage is required to provide sufficient torque for cell rotation during the capture of the cell by DEP.[23,31]

We developed a device that simplifies the capture of cancer cells and the measurement procedures of their dielectric properties, resulting in improved throughput for characterization. This technique is called continuous-flow ROT (cROT) because the rotational behavior of multiple cells can be measured continuously and simultaneously using a single device. The electrode locations for the cROT are schematically shown in Fig. 1(b). In the cROT, four sets of electrodes (#1–4) are arranged in the xz cross-section, as shown in Fig. 1(b), using two comb-shaped electrodes on the top and bottom of the device. This electrode structure can rotate the cells while maintaining the same torque between the electrodes because of the uniform electrode array on any plane in the xz cross-section. This structure allows the cells to flow in the y-direction in the microfluidic device while being aligned by DEP, with simultaneous measurement of their electrical properties by ROT. Additionally, cell manipulations other than pumping were not required. Therefore, the cROT has the potential to realize high-throughput measurements of the electrical properties of cancer cells. We believe that this would improve the throughput of conventional ROT devices.[29–31] Moreover, cROT has another advantage over conventional ROT in terms of the simpler device configuration. Conventional ROT devices for multiple cell analysis need an electrode array with at least three layers: wiring, insulation, and electrodes.[31] In contrast, the cROT device can be fabricated with minimal

alignment by combining single-layer electrode substrates with the same top and bottom patterns. Hence, the cROT device is simpler than that of conventional ROT.

This study was aimed at demonstrating the validity of the cROT concept for the simultaneous measurement of dielectric properties, particularly the permittivity of the cell membrane and the conductivity of the cell cytoplasm, with improved throughput. First, the rotational behavior of the cells was obtained without flow in the device to evaluate the performance of the cROT electrode structure (Fig. 1(b)) and measure the dielectric properties. Here, we introduced a procedure to acquire the properties based on image processing and confirmed that cROT could obtain the dielectric properties of HeLa cells similarly to conventional ROT. Second, the rotational behavior of cells continuously flowing between the electrodes in a microfluidic device was measured, and it was confirmed that the throughput of the cROT was significantly higher than that of the conventional ROT.

The remainder of this manuscript is organized as follows. Section 2 presents a conceptual study of the device, including the rotation mechanism and numerical results on the design of the device geometry. Section 3 presents the experimental setup. Section 4 presents an evaluation of the measurement performance of the cROT with and without flow conditions and discusses the throughput of cROT-based measurements of the dielectric properties of flowing cancer cells. Finally, section 5 summarizes the conclusions of this study.

2. Device concept and electric field simulation

The cROT device consists of three layers, with the upper and lower layers corresponding to the electrode substrates, as shown in Fig. 2. Each layer requires a single lithographic process for electrode fabrication; thus, complicated and cumbersome fabrication processes are not required for this device. Two comb-shaped electrodes are interdigitated on
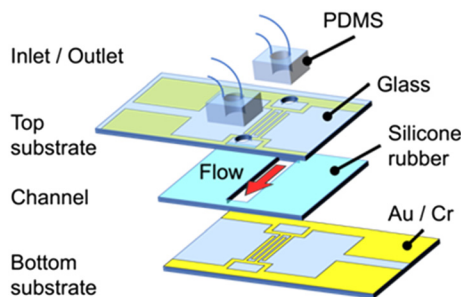
Fig. 2 Schematic of the cROT device, consisting of three layers: the top and bottom layers are electrode substrates, and the middle layer is the channel part. The red arrow in the channel part indicates the flow direction. The inlet and outlet are connected to tubing *via* PDMS blocks to allow cell pumping. Cells are analyzed while they flow through the channel.

each electrode substrate. A set of four electrodes in the *xz* cross-section is assembled by aligning the top and bottom electrodes, as shown in Fig. 1(b). The middle layer is the channel.

The electric field induced by the cROT was evaluated by numerical simulations to investigate the mechanism of cell

rotation between the electrodes. COMSOL Multiphysics® (v6.0) was utilized for conducting the three-dimensional numerical simulations in this study. The calculation domain was set at 160 μm × 160 μm × 50 μm (width (x) × depth (y) × height (z)) (see Fig. S1† in the ESI† for details on the simulation of the calculation domain, governing equations, and boundary conditions). The width of each electrode on the substrate is 30 μm, and the gaps between them are 50 μm. The channel height is also 50 μm. AC voltages of 1.5 V_{pp} and a frequency of 200 kHz were applied to the four electrodes, which were phase-shifted by 90° with respect to each other to induce ROT.

Fig. 3(a) shows the time-series electric field in the *xz* cross-section acquired by numerical simulation. The contour plot indicates the magnitude of the electric field and the arrows indicate the direction. Here, we focus on the area surrounded by a red frame located between the electrodes, where a cell is to be placed, to investigate the time-dependent variation of the electric field (bottom of Fig. 3(a)). T indicates the oscillation period of the applied electric field, and the time interval t in each field corresponds to $T/8$. Fig. 3(b) shows the ratio of the x-component (E_x) to the z-component (E_z) of the electric field, E_x/E_z, at the cell
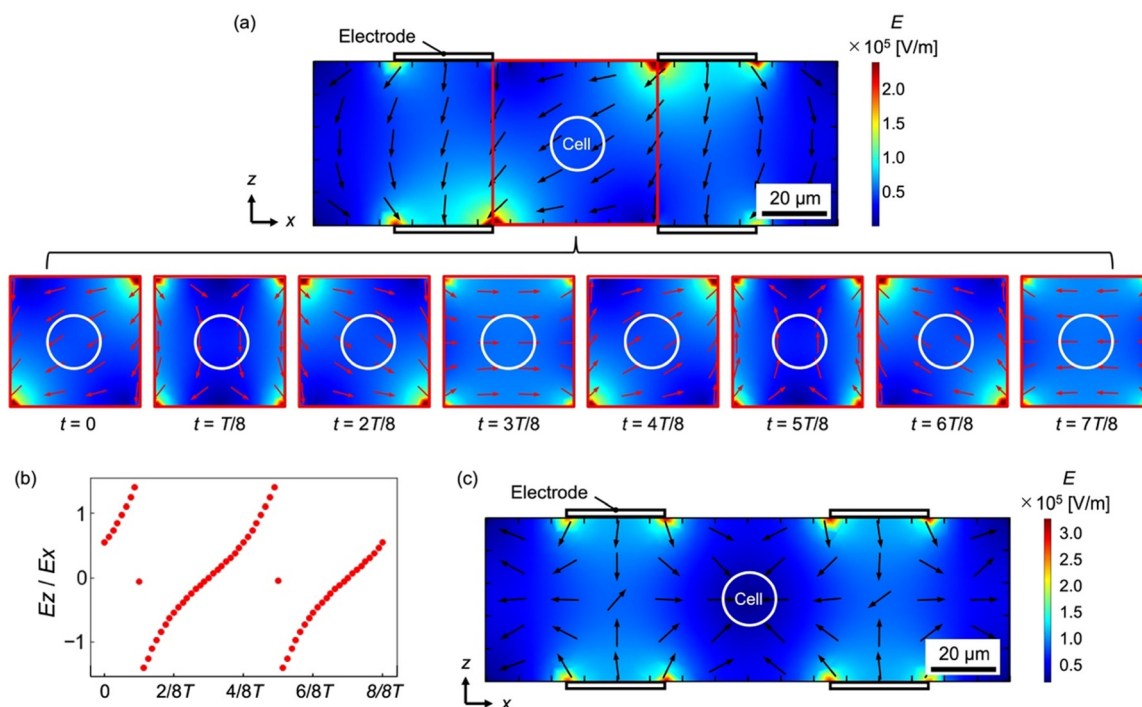

Fig. 3 Electric field distributions in the electrode structures of cROT obtained by numerical simulations. (a) 90°-phase-shifted AC voltage of 1.5 V_{pp} with 200 kHz frequency was applied to each electrode. The contour map and arrows indicate the magnitude and direction of the electric field, respectively. The time-series electric field in the area surrounded by the red box is shown in the bottom figure. The counterclockwise-rotating electric field gives a torque on the cell located between electrodes. This behavior of the rotating field is similar to that in conventional ROT, and it is confirmed that dielectric properties can be determined using this cROT electrode structure. (b) Time evolution of the E_z/E_x, which indicates the direction of the electric field's changes at the position of the cell (here, we assume that a cell is located 20 μm from the center of the electrodes). The periodicity of the trigonometric functions is confirmed, indicating that the electric field is rotating. (c) DEP voltages (1.5 V_{pp}, 20 kHz AC voltage with 180° phase shift) were applied to the four electrodes aligned in the *xz*-section. The contour map and the arrows indicate the magnitude of the electric field and the direction of the negative DEP force (direction of the electric field gradient), respectively. The DEP force acts in the direction away from the electrodes. This suggests that the cells are placed between the electrodes.

location, which indicates the direction of the torque. To determine the value of E_x/E_z equivalent to the tangent value in the rotating frame of reference, a distance of 20 μm from the center point of the electrode was utilized. Fig. 3(a) and (b) show that a rotating electric field is generated between the four electrodes in the calculation domain. Therefore, the cells placed between the electrodes can rotate because of the torque generated by the rotating electric field.

The angular velocity Ω of the cell receiving the torque from the rotating electric field is given as follows,

$$\Omega = \frac{\varepsilon_{\mathrm{m}}|E|^2}{2\eta} \mathrm{Im}[K^*(\omega)] \tag{2.1}$$

where ε_{m} is the permittivity of the medium, E is the electric field, η is the viscosity of the medium, ω is the frequency of the AC voltage, and the superscript * indicates complex numbers. Here, $K^*(\omega)$ is called the Clausius–Mossotti (CM) factor, which depends on the dielectric properties of the cell. Cancer cells consist of membranes, nuclei, and organelles. In this study, we modeled the cell as a single-shell model and treated it as a sphere composed of two layers: the membrane and the cytoplasm.[23,32] Using this model, we can evaluate the influence of various drugs on the membrane and cytoplasm of the cell as the dielectric properties change.[1,3,12,13] The CM factor $K^*(\omega)$ of the single-shell model is defined by eqn (2.2) using the permittivity of the membrane and cytoplasm of the cell in complex form, consisting of permittivity, conductivity, and oscillation frequency.[23,32] The permittivity of the cell $\varepsilon_{\mathrm{p}}^*$ is defined by eqn (2.3).

$$K^*(\omega) = \frac{\varepsilon_{\mathrm{p}}^* - \varepsilon_{\mathrm{m}}^*}{\varepsilon_{\mathrm{p}}^* + 2\varepsilon_{\mathrm{m}}^*} \tag{2.2}$$

$$\varepsilon_{\mathrm{p}}^* = \varepsilon_{\mathrm{mem}}^* \frac{\left(\frac{R}{R-d}\right)^3 + 2\frac{\varepsilon_{\mathrm{cyt}}^* - \varepsilon_{\mathrm{mem}}^*}{\varepsilon_{\mathrm{cyt}}^* + 2\varepsilon_{\mathrm{mem}}^*}}{\left(\frac{R}{R-d}\right)^3 - \frac{\varepsilon_{\mathrm{cyt}}^* - \varepsilon_{\mathrm{mem}}^*}{\varepsilon_{\mathrm{cyt}}^* + 2\varepsilon_{\mathrm{mem}}^*}} \tag{2.3}$$

Here, ε^* is the complex permittivity, the subscript p denotes the whole cell, m is the medium, mem is the cell membrane, and cyt is the cell cytoplasm. R is the cell radius and d is the membrane thickness, respectively. Eqn (2.1)–(2.3) indicate that the angular velocity of a cell depends on its dielectric properties contained in the CM factor. Therefore, the dielectric properties can be determined from the rotational behavior of the cell. Hence, it is possible to determine the dielectric properties of cancer cells using the device proposed in this study, in addition to the conventional ROT.

In the cROT, DEP was applied to cells simultaneously with ROT to place cancer cells between the electrodes. In DEP, when a dielectric particle is placed in an electric field, it polarizes and experiences an electrical force. DEP can be generated by applying 180°-phase-shifted AC voltages to the electrodes; thus, the same electrodes as those shown in Fig. 2 can be used. The DEP force acting on a particle F_{DEP}, is expressed as follows:

$$F_{\mathrm{DEP}} = 2\pi\varepsilon_{\mathrm{m}}R^3\mathrm{Re}[K^*(\omega)]\nabla|E|^2 \tag{2.4}$$

From eqn (2.4), the DEP force acts along the electric field gradient, and the sign of the real part of the CM factor determines its polarity. In the case of cancer cells, the real part of the CM factor is negative for an AC frequency of 10^0–10^5 Hz (and $>10^7$ Hz) and positive for 10^5–10^7 Hz.[32–34] Therefore, the negative DEP force on the cell works toward a smaller electric field along the gradient when the real part of the CM factor is negative. In contrast, when the real part is positive, the DEP force works toward an area with a larger electric field along the gradient.

Fig. 3(c) shows the magnitude of the electric field and the direction of the electric field gradient when a negative DEP is induced. Here, 180°-phase-shifted AC voltages of 1.5 V_{pp} and a frequency of 20 kHz were applied to the electrodes of the same calculation model (Fig. S1†), to arrange the cells between the electrodes. As shown in Fig. 3(c), the electric field increases near the electrode and decreases further away from the electrode. Thus, the cells in the device were placed between the electrodes because the DEP force worked on the cells in the direction away from the electrodes, as indicated by the arrows in Fig. 3(c). Because the DEP force works even if flow occurs in the device, cells are transported from upstream to downstream, maintaining their positions between the electrodes when the flow direction is perpendicular to the xz-plane, i.e. along the y-direction. Therefore, the cROT can be achieved under these conditions.

To increase the ROT torque and DEP forces acting on the cancer cells, the electrode gap (channel height) was adjusted appropriately in the actual device. Numerical simulations were also used to investigate the effects of the device geometry on the ROT and DEP. Fig. 4 shows that the intensity of the electric field increases near the electrodes. Additionally, from eqn (2.1), the angular velocity of the cell increases with the field intensity. Since the typical diameter of the cancer cells to be measured in this study ranges from 12 to 20 μm, the electric field at the center of the electrode for a 20 μm-sized cell (the location corresponding to the dashed line shown in Fig. 4) was compared. Because cells come into contact with the top or bottom of the channel when the channel height is 20 μm, the minimum spacing of the electrode and channel was set to 30 μm. Electric field simulations were performed for electrode gaps and channel heights of 30, 40, and 50 μm. A voltage of 1.5 V_{pp} at a frequency of 200 kHz was applied. The calculation conditions, excluding the channel height, were the same as those used in the previous simulation. Fig. 4(b) indicates that the electric field at the floating position of the cell increases as the electrode gap decreases, and the electric field at a gap of 30 μm is approximately double that at 50 μm. When the channel height is 30 μm, the rotation speed of the cell is four times faster than that at a height of 50 μm, based on eqn (2.1). The smaller the electrode gap, the easier it is to measure the rotational movement of the cell. The magnitude of the DEP force required to align the cells between the electrodes also depends on the electric field, based on eqn (2.3). Therefore, a
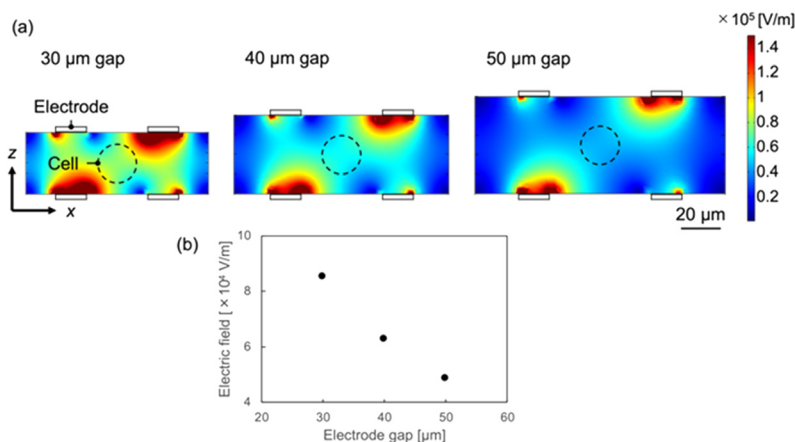
Fig. 4 (a) Simulation results of the electric field obtained in different electrode gaps of 30, 40, and 50 μm. (b) The relationship between the electrode gap (channel height) and the magnitude of the electric field obtained at the position of the cell (20 μm in diameter from the center of the electrodes). The smaller the electrode gap, the larger the magnitude of the electric field.

smaller electrode gap enables a stronger DEP force to work on the cells, and the cell is held more stably between the electrodes. From these results, both the electrode gap and channel height in this study were set to 30 μm.

3. Experimental

3.1. Device fabrication

For the cROT device used in this study (the schematic is illustrated in Fig. 2), Au/Cr (80/10 nm thickness) sputter-coated glass substrates were used as the electrode substrates. The electrodes were patterned by wet-etching using Au and Cr etchants. The top and bottom substrates have the same electrodes. The non-etched area was protected by coating it with a positive photoresist (7790G-27cP, JSR). After electrode patterning, inlet and outlet holes were drilled into the top substrate, and the channel was attached to the bottom substrate. The channel was made of a silicone sheet (ARFS-5030, Asahi Rubber) with a width, length, and height of 3 mm, 10 mm, and 30 μm, respectively. Perfluoroalkoxy (PFA) tubes were connected to the inlet and outlet holes and were connected *via* polydimethylsiloxane (PDMS) blocks.

3.2. Cell preparation

HeLa cells, a well-known human cervical cancer cell line, were used in this study. The cells were supplied by the Faculty of Pharmaceutical Sciences in our university and were cultured in 5% CO_2 at 37 °C. The HeLa cells were removed from the culture dish using trypsin because they are adhesive cells. The cells were then transferred to the working medium for DEP and ROT at a density of 1.5×10^6 cells per mL after the medium was removed by centrifugation. The working medium was a buffer solution with controlled conductivity, osmotic pressure, and density. The medium was prepared by mixing sucrose, HEPES, Percoll, and ultrapure water. The conductivity of the solution was set to 0.038 S m^{-1} to prevent Joule heating, while the electric fields for ROT and DEP were applied. The osmotic pressure was maintained at 280 mOsm L^{-1} to prevent cell condensation or rupture. The solution density was set to 1.06 g cm^{-3} to prevent the cells from settling.

3.3. Experimental setup

Bright-field observations were used to analyze the rotational behavior of the cells. The schematic of the whole experimental setup is shown in the ESI† (Fig. S2). The observation system consisted of an imaging system with an inverted microscope (TE-2000, Nikon). A 20× objective lens (S Plan Fluor ELWD 20×, NA = 0.45, Nikon) and a scientific CMOS camera (2304 × 2304 pixels, 23.27 fps, ORCA Fusion, Hamamatsu Photonics) were used. The spatial resolution of the image acquisition system was 6.5 μm/pixel. The imaging area was 748.8 μm × 748.8 μm. Continuous light-emitting diode (LED) light (KL-LED 2500, SCHOTT) was used as the illumination source. A syringe pump (Pump 11 Elite, HARVARD) was used to infuse the cells at a constant flow rate. The ROT and DEP signals were superimposed using arbitrary waveform creation software (ArbConnection, Tabor Electronics), and the signals were applied to the device *via* a function generator (WW2074, Tabor Electronics). Using these systems, successive images of rotating cells were acquired and analyzed to determine the angular velocity by image processing. The details of the image processing are described later.

4. Results and discussion

4.1. Evaluation of the dielectric property measurement performance of the cROT electrode structure

To evaluate the validity of our device for dielectric property measurements, the rotational movement of cells without flow was observed using the fabricated device. An AC voltage of 1.5 V$_{\text{PP}}$ was applied at 20 kHz for DEP and over the range from 50 kHz to 1 MHz for ROT. HeLa cells were infused into
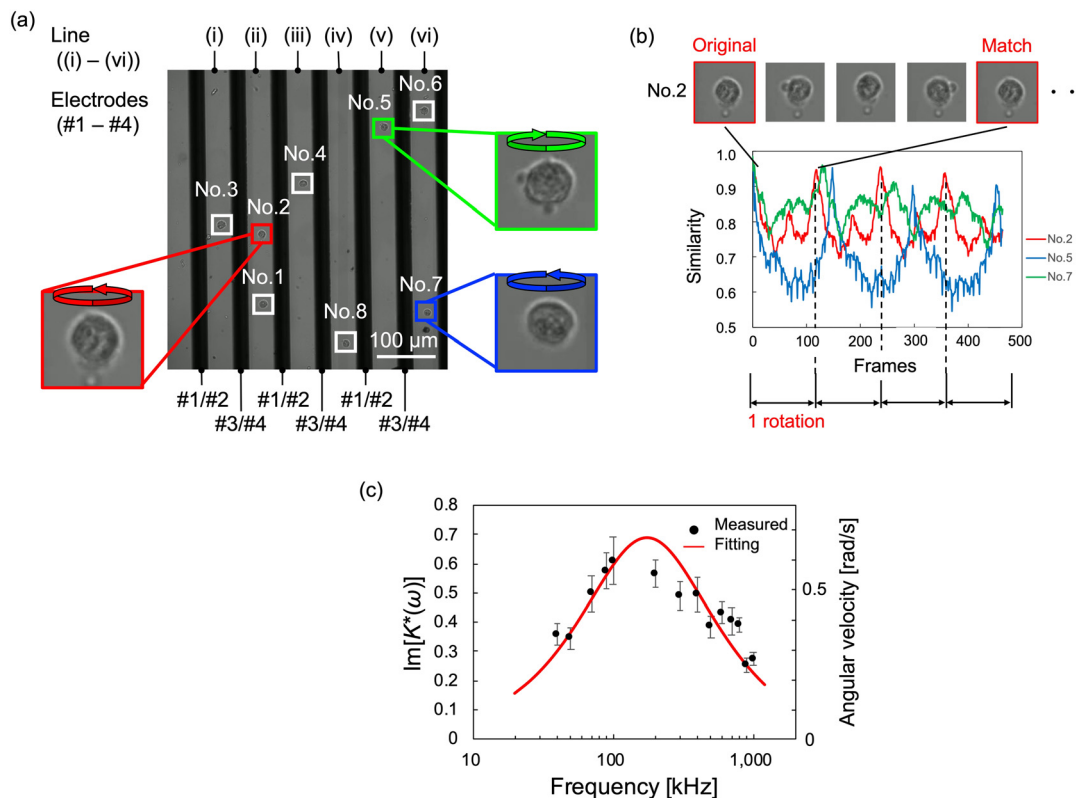
Fig. 5 Observed image of rotating HeLa cells and their dielectric properties using the cROT electrode without flow. (a) Multiple HeLa cells were arranged, and they rotated between the electrodes while maintaining their positions. The measurement positions (i)–(vi) are surrounded by four electrodes (#1–4; these numbers correspond to those shown in Fig. 1(b)), creating a uniform rotating electric field. Depending on the electrodes and line positions, the rotation direction of the cell is different between odd positions ((i), (iii), (v)) and even positions ((ii), (iv), (vi)). The applied voltage signal is a superposition of 1.5 V_{pp} with 100 kHz for ROT and 5.0 V_{pp} with 20 kHz for DEP. (b) Examples of rotation analysis of each cell. The rotation speed was determined by image processing. The image processing used template matching to compare the image of frame 0 (template image) with the images of other successive frames (compared images). The comparison results were output as a similarity, confirming the periodicity corresponding to the rotational behavior. Therefore, the rotation speed of the cells was calculated from the periodicity of the similarity. (c) ROT spectrum obtained from HeLa cells. Dielectric properties were calculated by curve fitting. Since the dielectric properties are a parameter included in the CM factor, the dielectric properties were estimated by the least-squares method for the imaginary part of the CM factor calculated from the measured angular velocity. The error bars in the figure correspond to the standard error ($n \approx 10$).

the device and were randomly distributed throughout the channel. Fig. 5(a) shows an instantaneous image of HeLa cells arranged by DEP between the electrodes and rotated by the ROT. During this experiment, we simultaneously obtained the rotational movements of 4–11 HeLa cells from successive images. In Fig. 5(a), the dark areas correspond to the electrodes, and all the cells can be found in the bright areas between the electrodes, which means that the location of the cells is well controlled by negative DEP. Cells near the electrodes received a force directed away from the electrodes by DEP and were gradually and automatically aligned between the electrodes. Each cell rotated in the direction vertical to the observation plane between the electrodes, as predicted. The rotational axis of the cell was parallel to the electrode. In the cROT, a rotating electric field was generated using four electrodes (#1–4). Two of the four electrodes were shared with neighboring electrode pairs in the electrode structure used in this study. Therefore, the rotational direction of the electric field was reversed according to the arrangement of the electrodes, and we observed that the cells

rotated in the clockwise direction at positions (i), (iii), and (v) and in the counterclockwise direction at positions (ii), (iv), and (vi), as shown in Fig. 5(a) and Video S1.†

Subsequently, the angular velocity of each rotating cell was determined using image processing. Template matching utilizing OpenCV was employed to analyze the rotational speed. The first frame of each cell image was employed as the template image, and the successively obtained images in other frames were used for comparison. The similarity between the template and compared images was calculated as the normalized correlation coefficient, and the time variation of the similarity in the successive images for each cell was investigated to determine the rotational periodicity. The validity of the rotation analysis method was preliminary evaluated by artificial cell images with virtual rotation, and the accuracy of the angular velocity was less than 0.25%.

The time-series similarity among cell No. 2, 5, and 7 depicted in Fig. 5(a) was obtained, as shown in Fig. 5(b). During rotation, the similarity values show periodic behavior with decreasing and increasing values; when a cell rotates

once, the similarity value approaches unity. Notably, the similarity is equal to one when the complete cell image matches the template and compared images, but in the actual case, the maximum value of the similarity after a rotation is smaller than one since the appearance is not exactly the same because of the slight change in the background. The period of similarity for the rotating cells (shown in Video S2 in the ESI†) is consistent with the cycle of cell rotation. Therefore, it was possible to determine the rotational speed of each cell using a periodicity analysis based on template matching.

The image processing indicated above was applied to all the observed rotating cells, and the angular velocity of the cells was obtained for each frequency of the applied voltage as shown in Fig. 5(c). The imaginary part of the CM function was calculated using eqn (2.1)‐ based on the angular velocities which were acquired from image processing. Then the dielectric properties, ε_{mem} and σ_{cyt} in eqn (2.2), were estimated using the least-squares method. In this calculation, we obtained two parameters, ε_{mem} and σ_{cyt}, among the four variables in eqn (2.3) because the other two parameters, σ_{mem} and ε_{cyt}, showed little change in the frequency range normally used in ROT.[13] The fixed parameters in the least-squares fitting are shown in Table 1.[30] The obtained values of ε_{mem} and σ_{cyt} were 7.34 ± 0.75 (±standard error, S.E.) and 1.07 ± 0.11 (±S.E.) S m^{-1}, respectively. The dielectric properties of HeLa cells measured by ROT have been reported as ε_{mem} = 7.40–19.78 and σ_{cyt} = 0.36–1.25, with a relatively wide range of variation.[13,30,35] In our previous study,[34] the dielectric properties of HeLa cells measured using a ROT device based on the concept shown in Fig. 1(a) were 10.20 ± 1.74 (±S.E.) and 1.01 ± 0.13 (±S.E.) S m^{-1}. The variation in these measurement values between the present results and those obtained in our previous study is within the variation of the reported results; therefore, the measurement results obtained in this study are considered reasonable. Therefore, it can be said that the dielectric properties of cancer cells could be measured using the electrode structure in our developed device based on the cROT concept (shown in Fig. 1(b)).

Because multiple cells placed between the electrodes can be measured simultaneously in our device, these measurement schemes, which rely on the cROT electrode structure, are expected to improve the throughput of dielectric property measurements. Furthermore, in this experiment, cells, except for aggregated cells (approximately 10% of the observed cells), rotated between the electrodes; thus, the cell capture rate was achieved at approximately 90% of the infused cells in the device. This implies the potential

of cROT to improve the low capture rate, which is an issue in conventional ROTs.[29,31]

4.2. Continuous-flow measurement of dielectric properties of cancer cells by cROT

As mentioned above, the cROT has the potential to improve measurement throughput by observing the rotational behavior of the cells under continuous flow. The electrodes used in section 4.1 automatically align the infused cells in the channel toward the area between the electrodes, and the rotation behavior of the cells anywhere in the entire field of view of the microscope could be observed. Therefore, the cells aligned between the electrodes can be measured under flow conditions. The time for the cells to flow through the observation area must be sufficient to analyze their rotation. Here, the flow rate of the syringe pump was set to 7.5 μL h^{-1}, and the flow velocity of the cells in the device became 20 μm s^{-1}. This allowed an observation time of approximately 30 s, which was equivalent to the period shown in Fig. 5(b).

Under these experimental conditions, the dielectric properties of HeLa cells were measured using the cROT. The device and applied voltage conditions are the same as in section 4.1. Fig. 6(a) shows an example of the images acquired for rotating cells while flowing at t = 0 s and 10 s at a frequency of 100 kHz. Flowing cells were automatically detected using in-house image processing software and are surrounded by white boxes, as shown in Fig. 6(a) and Video S3.† The cells flowed between electrodes at a uniform speed. Here, the detected objects (cells surrounded by white boxes in Fig. 6(a)) with a width of 20 μm or larger were determined as aggregated cells based on the size of the detected cells, and they were excluded from the analysis. Thus, more than 30 vertically rotating cells were detected in the observed area, and it was possible to analyze them simultaneously.

The rotational behavior of the detected cells was analyzed using the image processing method described in section 4.1. Some detected cells could not be analyzed for angular velocity owing to low image quality or noise, and at most, 32 cells could be measured simultaneously. Fig. 6(b) shows the typical time-series similarity of the cells in this experiment. In addition, in the cROT with flow, a periodicity in similarity was observed. The angular velocities of the cells were then measured. The dielectric properties, ε_{mem} and σ_{cyt}, calculated from the ROT spectrum shown in Fig. 6(c) were 9.13 ± 1.02 (±S.E.) and 0.93 ± 0.10 (±S.E.) S m^{-1}, respectively. The dielectric properties of the HeLa cells obtained by conventional ROT and cROT are summarized in Table 2. As described in section 4.1, this result is within a reasonable value considering the range of variation of previously reported properties.[13,30,35] Therefore, it is possible to say that the cROT can properly measure the dielectric properties under continuous flow conditions. Additionally, ε_{mem} and σ_{cyt} measured in the cROT device with and without flow can be regarded as equivalent, and it is considered that the analysis

Table 1 The fixed parameters used for curve fitting

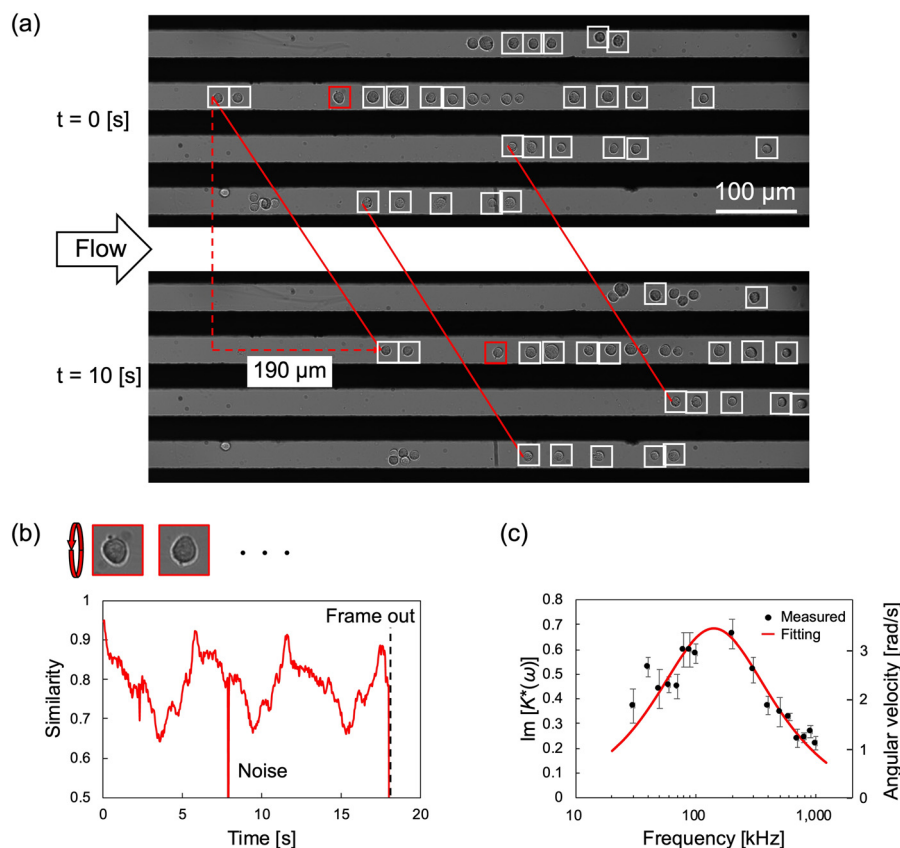|	
Medium permittivity (ε_m) [–][30]	80
Medium conductivity (σ_m) [S m^{-1}]	0.038
Medium viscosity (η) [Pa s]	3.0×10^{-3}
Membrane conductance (G_{mem}) [S m^{-2}][30]	0.95
Cytoplasm permittivity (ε_m) [–][30]	60

Fig. 6 Dielectric property measurement of HeLa cells by cROT under flow conditions. (a) Multiple HeLa cells aligned between electrodes by DEP showed rotational behavior by ROT. Since a uniform electric field was formed between the electrodes in the flow direction, the cells continued rotating along the flow direction between the electrodes. All observed cells flowed with almost the same velocity of 20 μm s^{-1}. Since the length of the observation area is 748.8 μm, the cells to be measured are automatically replaced in $\approx$40 s. The applied voltage signal is a superposition of 1.5 V_{pp} with 800 kHz for ROT and 1.5 V_{pp} with 20 kHz for DEP. (b) The rotational behavior of HeLa cells measured by cROT was analyzed by image processing as in Fig. 5(b). The same periodic similarity as that shown in Fig. 5(b) is obtained under the flow conditions, and the angular velocity of the cell could be calculated. (c) ROT spectrum obtained by cROT. Dielectric properties were calculated by curve fitting using the angular velocity of the cells obtained by image processing. The error bars correspond to the standard error ($n \approx 30$).

Table 2 Dielectric properties of HeLa cells measured by ROT, cROT (w/o flow), and cROT (w/ flow)

	ROT[34]	cROT (w/o flow)	cROT (w/ flow)
Membrane permittivity (ε_{mem}) [−]	10.20 ± 1.74	7.34 ± 0.75	9.13 ± 1.02
Cytoplasm conductivity (σ_{cyt}) [S m^{-1}]	1.01 ± 0.13	1.07 ± 0.11	0.93 ± 0.10

for the flowing cells has no influence on the dielectric property measurements.

Finally, the measurable number of cells per unit time (cells per h) was evaluated as the throughput of dielectric property measurements. The throughput was calculated based on the number of cells that could be captured simultaneously and the measurement time. In addition, the throughput was compared with those obtained in previous

Table 3 Throughputs in measurement of dielectric properties of cancer cells using ROT and cROT

	Electrodes [−]	Cells [−]	Measurement [h]	Throughput [cells per h]
Conventional ROT[13,23,34,36]	1	1	0.05−0.08	12−20
Tsuchiya et al.[31]	36	5	0.05−0.08	60−100
Suzuki et al.[37]	225	70	0.25	420
Keim et al.[30]	39	39	0.025	600
cROT (this study)	13	32	0.011	2700

studies. These values are summarized in Table 3. Here, the measurement time was the sum of the time required to obtain the ROT spectra and the time required to introduce and replace cells. In the conventional ROT, the process of capturing a new cell at the measurement location where the rotating electric field is induced must be repeated if the device can measure only a single cell.[13,23,34,36] The time required to acquire the ROT spectra was approximately 3 min, and the cell replacement time was approximately 5 min; thus, the throughput was calculated to be 12–20 cells per h.

Some studies have reported the simultaneous measurement of the dielectric properties of cells with improved throughput using an array of electrodes. Tsuchiya et al.[31] fabricated a 6 × 6 array of pillar-shaped electrodes that could simultaneously measure the rotational behaviors of multiple beads. They indicated that the measurements could be conducted simultaneously at five locations. Suzuki et al.[37] fabricated 225 sets of electrode arrays using microband electrodes placed above and below the microwells; the cells were captured in microwells in 10–15 min, and 70 cells were measured simultaneously. Keim et al.[30] developed a DEP actuator that could independently capture and release individual cells. This technique enabled 100% cell capture at 39 measurement positions and reduced the cell replacement time to 12 s. These improvements in cell manipulation have increased the measurement throughput to 600 cells per h.

Compared to the previous ROT studies presented above, the cROT developed in this study allows the cell replacement time to be ignored by introducing a continuous flow for cell replacement and measurement. This is because the cells automatically flowed into and out of the observation area. The cells passed through the 748.8 μm length of the observation area at a flow velocity of 20 μm s^{-1} so that the ROT spectra could be obtained during this 40 s. For this case, the measurement throughput of cROT is calculated to be 2700 cells per h. Although the throughput itself is not as high as the impedance flow cytometry (IFC),[38,39] ROT measurement under continuous flow in the proposed cROT has the potential to realize a significantly higher throughput of dielectric property measurements in cancer cells.

When the rotational behavior of cancer cells under continuous flow is measured, cells that settle and adhere to the substrate surface cannot be measured. In addition, cells that adhere to the substrate aggregate with the flowing cells, clogging the channel. In our study, the number of cells adhering to the substrate was approximately 10–20% of all flowing cells. The adhesion rate of cells can be improved by appropriate surface treatments or coatings, and the throughput can be further improved by increasing the number of measurable cells. Furthermore, the number of cells that can be observed is limited by current imaging systems, particularly by the resolution and frame rate of the camera. Further improvement in the measurement throughput is expected by capturing a wider domain with higher spatial resolution and frame rates.

Conclusions

In this study, we proposed a new electrical cell characterization approach, continuous-flow electrorotation (cROT), for the high-throughput measurement of the dielectric properties of cancer cells by successive analysis of flowing cells using an interdigitated electrode embedded on the top and bottom substrates of the device. The dielectric properties obtained with and without flow were similar to those obtained by conventional ROT, confirming that the new electrode structure and continuous analysis did not degrade the measurement performance. In addition, the electrode geometry in the cROT enables an increased number of cells to be measured simultaneously and reduces the time required for cell replacement, resulting in a significant increase in throughput. Although there is room for improvement in the measurement throughput using the cROT, this concept facilitates the measurement of the dielectric properties of cancer cells. We believe that the concept of the cROT is valuable for the development of cancer diagnostic applications that utilize its dielectric properties.

Author contributions

KY – investigation, fabrication, writing – original draft; YI – writing – review& editing; MM – conceptualization, methodology, writing – review& editing, supervision, funding acquisition.

Conflicts of interest

There are no conflicts to declare.

Acknowledgements

References

1 W. Si, J. Shen and W. Fan, The role and mechanisms of action of microRNAs in cancer drug resistance, *Clin. Epigenet.*, 2019, **11**, 25.
2 Y. Sun, J. Campisi, C. Higano, T. M. Beer, L. Coleman, L. True and P. S. Nelson, Treatment-induced damage to the tumor microenvironment promotes prostate cancer therapy resistance through WNT16B, *Nat. Med.*, 2012, **18**, 1359–1368.

3 D. B. Longley and P. G. Johnston, Molecular mechanisms of drug resistance, *J. Pathol.*, 2005, **205**(2), 275–292.

4 M. M. Gottesman, Mechanisms of cancer drug resistance, *Annu. Rev. Med.*, 2002, **53**, 615–627.

5 J. Fares, M. Y. Fares, H. H. Khachfe, H. A. Salhab and Y. Fares, Molecular principles of metastasis: a hallmark of cancer revisited, *Signal Transduction Targeted Ther.*, 2020, **5**, 28.

6 Y. Suhail, M. P. Cain, K. Vanaja, P. A. Kurywchak, A. Levchenko, R. Kalluri and Kshitiz, Systems biology of cancer metastasis, *Cell Syst.*, 2019, **9**(2), 109–127.

7 T. Todenhöfer, W. J. Struss, R. Seiler, A. W. Wyatt and P. C. Black, Liquid biopsy-analysis of circulating tumor DNA (ctDNA) in bladder cancer, *Bladder Cancer*, 2018, **4**(1), 19–29.

8 K. E. Henson, R. Brock, J. Charnock, B. Wickramasinghe, O. Will and A. Pitman, Risk of suicide after cancer diagnosis in England, *JAMA Psychiatry*, 2019, **76**(1), 51–60.

9 H. M. Huttanus, T. Vu, G. Guruli, A. Tracey, W. Carswell, N. Said, P. Du, B. G. Parkinson, G. Orlando, J. L. Robertson and R. S. Senger, Raman chemometric urinalysis (Rametrix) as a screen for bladder cancer, *PLoS One*, 2020, **15**(8), e0237070.

10 M. M. Koo, C. von Wagner, G. A. Abel, S. McPhail, W. Hamilton, G. P. Rubin and G. Lyratzopoulos, The nature and frequency of abdominal symptoms in cancer patients and their associations with time to help-seeking: evidence from a national audit of cancer diagnosis, *J. Public Health*, 2018, **40**(3), e388–e395.

11 Z. Çağlayan, Y. D. Yalçın and H. Külah, A prominent cell manipulation technique in BioMEMS: Dielectrophoresis, *Micromachines*, 2020, **11**(11), 990.

12 A. Han, L. Yang and A. B. Frazier, Quantification of the heterogeneity in breast cancer cell lines using whole-cell impedance spectroscopy, *Clin. Cancer Res.*, 2007, **13**(1), 139–143.

13 L. Huang, P. Zhao and W. Wang, 3D cell electrorotation and imaging for measuring multiple cellular biophysical properties, *Lab Chip*, 2018, **18**, 2359–2368.

14 M. Hussein, F. Awwad, D. Jithin, H. E. Hasasna, K. Athamneh and R. Iratni, Breast cancer cells exhibits specific dielectric signature in vitro using the open-ended coaxial probe technique from 200 MHz to 13.6 GHz, *Sci. Rep.*, 2019, **9**, 4681.

15 X. Yu, Y. Sun, K. Cai, H. Yu, D. Zhou, D. Lu and S. X. Xin, Dielectric properties of normal and metastatic lymph nodes ex vivo from lung cancer surgeries, *Bioelectromagnetics*, 2020, **44**(2), 148–155.

16 M. Guardiola, S. Buitrago, G. Fernández-Esparrach, J. M. O'Callaghan, J. Romeu, M. Cuatrecasas, H. Córdova, M. Á. G. Ballester and O. Camara, Dielectric properties of colon polyps, cancer, and normal mucosa: Ex vivo measurements from 0.5 to 20 GHz, *Med. Phys.*, 2018, **45**(8), 3768–3782.

17 L. L. Crowell, J. S. Yakisich, B. Aufderheide and T. N. G. Adams, Electrical impedance spectroscopy for monitoring chemoresistance of cancer cells, *Micromachines*, 2020, **11**(9), 832.

18 L. F. E. Huerta-Nuñez, G. Gutierrez-Iglesias, A. Martinez-Cuazitl, M. M. Mata-Miranda, V. D. Alvarez-Jiménez, V. Sánchez-Monroy, A. Golberg and C. A. González-Díaz, A biosensor capable of identifying low quantities of breast cancer cells by electrical impedance spectroscopy, *Sci. Rep.*, 2019, **9**, 6419.

19 A. Alazzam, B. Mathew and F. Alhammadi, Novel microfluidic device for the continuous separation of cancer cells using dielectrophoresis, *J. Sep. Sci.*, 2017, **40**, 1193–1200.

20 S. Ayala-Mar, V. H. Perez-Gonzalez, M. A. Mata-Gomez, R. C. Gallo-Villanueva and J. Gonzalez-Valdez, Electrokinetically driven exosome separation and concentration using dielectrophoretic-enhanced PDMS-based microfluidics, *Anal. Chem.*, 2019, **91**(23), 14975–14982.

21 J. M. Lewis, A. D. Vyas, Y. Qiu, K. S. Messer, R. White and M. J. Heller, Integrated analysis of exosomal protein biomarkers on alternating current electrokinetic chips enables rapid detection of pancreatic cancer in patient blood, *ACS Nano*, 2018, **12**, 3311–3320.

22 S. D. Ibsen, J. Wright, J. M. Lewis, S. Kim, S. Y. Ko, J. Ong, S. Manouchehri, A. Vyas, J. Akers, C. C. Chen, B. S. Carter, S. C. Esener and M. J. Heller, Rapid isolation and detection of exosomes and associated biomarkers from plasma, *ACS Nano*, 2017, **11**(7), 6641–6651.

23 S. I. Han, Y. D. Joo and K. H. Han, An electrorotation technique for measuring the dielectric properties of cells with simultaneous use of negative quadrupolar dielectrophoresis and electrorotation, *Analyst*, 2013, **138**, 1529–1537.

24 U. Lei, P. H. Sun and R. Pethig, Refinement of the theory for extracting cell dielectric properties from dielectrophoresis and electrorotation experiments, *Biomicrofluidics*, 2011, **5**(4), 044109.

25 Y. J. Lo, U. Lei, K. Y. Chen, Y. Y. Lin, C. C. Huang, M. S. Wu and P. C. Yang, Derivation of the cell dielectric properties based on Clausius-Mossotti factor, *Appl. Phys. Lett.*, 2014, **104**(11), 113702.

26 C. I. Trainito, D. C. Sweeney, J. Čemažar, E. M. Schmelz, O. Français, B. L. Pioufle and R. V. Davalos, Characterization of sequentially-staged cancer cells using electrorotation, *PLoS One*, 2019, **14**(9), e0222289.

27 T. Michálek, A. Bolopion, Z. Hurák and M. Gauthier, Electrorotation of arbitrarily shaped micro-objects: modeling and experiments, *IEEE ASME Trans. Mechatron.*, 2020, **25**(2), 828–836.

28 L. Huang, W. He and W. Wang, A cell electro-rotation micro-device using polarized cells as electrodes, *Electrophoresis*, 2019, **40**(5), 784–791.

29 S. Kawai, M. Suzuki, S. Arimoto, T. Korenagab and T. Yasukawa, Determination of membrane capacitance and cytoplasm conductivity by simultaneous electrorotation, *Analyst*, 2020, **145**, 4188.

30 K. Keim, M. Z. Rashed, S. C. Kilchenmann, A. Delattre, A. F. Goncalves, P. Ery and C. Guiducci, On-chip technology for single-cell arraying, electrorotation-based analysis and selective release, *Electrophoresis*, 2019, **40**, 1830–1838.

31 T. Tsuchiya, Y. Okamoto, F. Marty, A. Mizushima, A. Tixier-Mita, O. Français, B. L. Pioufle and Y. Mita, Two-dimensionally arrayed double-layer electrode device which

enables reliable and high-thoroughput electrortation, *Proc. IEEE 34th Int. Conf. Micro Electro Mech. Syst.*, 2021, 486–489.

32 R. Pethig, Review Article—Dielectrophoresis: Status of the theory, technology, and applications, *Biomicrofluidics*, 2010, **4**, 022811.

33 C. P. Jen and T. W. Chen, Selective trapping of live and dead mammalian cells using insulator-based dielectrophoresis within open-top microstructures, *Biomed. Microdevices*, 2009, **11**, 597–607.

34 K. Yoda, Y. Sasaki, K. Yamamoto, Y. Ichikawa and M. Motosuke, Label-free dielectrophoretic separation of cancer cell by drug resistance, *Proc. 25th Int. Conf. Miniaturized Syst. Chem. Life Sci. (MicroTAS 2021)*, 2021, pp. 249–250.

35 W. Liang, X. Yang, J. Wang, Y. Wang, W. Yang and L. Liu, Determination of dielectric properties of cells using AC electrokinetic-based microfluidic platform: a review of recent advances, *Micromachines*, 2020, **11**, 513.

36 M. Cristofanilli, G. De Gasperis, L. Zhang, M. C. Hung, P. R. C. Gascoyne and G. N. Hortobagyi, Automated electrorotation to reveal dielectric variations related to HER-2/neu overexpression in MCF-7 sublines, *Clin. Cancer Res.*, 2002, **8**, 615–619.

37 M. Suzuki, S. Kawai, C. F. Shee, R. Yamada, S. Uchida and T. Yasukawa, Development of a simultaneous electrorotation device with microwells for monitoring the rotation rates of multiple single cells upon chemical stimulation, *Lab Chip*, 2023, **23**, 692–701, Advanced article.

38 X. Luan, P. Liu, D. Huang, H. Zhao, Y. Li, S. Sun, W. Zhang, L. Zhang, M. Li, T. Zhi, Y. Zhao and C. Huang, piRT-IFC: Physics-informed real-time impedance flow cytometry for the characterization of cellular intrinsic electrical properties, *Microsyst. Nanoeng.*, 2023, **9**, 77.

39 Y. Feng, L. Huang, P. Zhao and W. Wang, A microfluidic device integrating impedance flow cytometry and electric impedance spectroscopy for high-efficiency single-cell electrical property measurement, *Anal. Chem.*, 2019, **91**, 15204–15212.